

Preparation of barium strontium titanate $\text{Ba}_{1-x}\text{Sr}_x\text{TiO}_3$ ($0 \leq x \leq 0.2$) single-crystal nanorods by a novel combined method

Wanquan Jiang^{a,*}, Xiuqing Gong^a, Zuyao Chen^{a,b}, Yuan Hu^b,
Xianzhou Zhang^c, Xinglong Gong^c

^a Department of Chemistry, University of Science and Technology of China, Hefei, Anhui 230026, PR China

^b State Key Laboratory of Fire Science, University of Science and Technology of China, Hefei, Anhui 230026, PR China

^c Department of Mechanics and Mechanical Engineering, University of Science and Technology of China, Hefei, Anhui 230026, PR China

Received 14 November 2005; received in revised form 18 January 2006; accepted 7 February 2006

Available online 18 April 2006

Abstract

An ultrasonic irradiation method was applied to the sol/gel synthesis of the single-crystal cubic barium strontium titanate $\text{Ba}_{1-x}\text{Sr}_x\text{TiO}_3$ ($0 \leq x \leq 0.2$). The characteristics of the composites were examined by X-ray diffraction, thermogravimetric analysis, differential thermal analysis, transmission electron microscopy and high-resolution transmission microscopy. The diameters and lengths of typical resultant $\text{Ba}_{0.8}\text{Sr}_{0.2}\text{TiO}_3$ are in the range of 70–100 nm and 650–1000 nm, respectively. In addition, the stoichiometric sonogel formation and its heat-treatment process, the relationship between x of $\text{Ba}_{1-x}\text{Sr}_x\text{TiO}_3$ and the crystal structure, the relationship between synthesis condition of sonogel and morphology have been discussed.

© 2006 Elsevier B.V. All rights reserved.

PACS: 61.66.F

Keywords: Nanorods; Barium strontium titanate; Ultrasonic radiation; Sol–gel method; Sonogel

1. Introduction

During the past decade, low-dimensional nanostructured materials have received considerable attention due to their potential applications in nano-electronics, optoelectronics, chemical sensors, catalysts, biological medicines, etc [1–5]. Transition metal oxides with cubic-perovskite structure are a particularly interesting class of materials, which exhibit a variety of unique electronic, magnetic, and optical properties. As a typical representative, barium strontium titanate (BST) is a kind of useful electronic ceramic material with fine performance and high dielectric constant, especially in the application of sensitive components and high voltage capacitors. Moreover, the substitution of barium

by strontium in barium titanate can improve the properties such as lowering the temperature of ferroelectric transformation, increasing dielectric constant, lowering dielectric dissipation and elevating pyroelectric coefficient [6–11].

There have been many methods developed for preparing BST materials, including conventional mixing and calcining method [12–14], coprecipitating method [15,16], organic compounds method [17], hydrothermal synthesis [18,19] and sol–gel process [20,21]. Among these methods, the sol–gel method has many promising characteristics such as lower operating temperature, easier control of the process and higher purity of the products. When the conventional sol–gel method or ultrasonic radiation was used for preparing low-dimensional nanomaterials, the templates are necessary as assistants in general [22–25]. The preparation of low-dimensional BST nanomaterials has already been reported using decomposition of divalent metallic alkoxide precursors [26] and laser heated pedestal growth [27], etc.

* Corresponding author. Fax: +86 551 3601592.

E-mail addresses: jiangwq@ustc.edu.cn (W. Jiang), xqgong@mail.ustc.edu.cn (X. Gong).

Herein, a simple combined ultrasonic radiation and conventional sol/gel method is employed to prepare low-dimensional BST nanomaterials. The combined method can easily produce barium strontium titanate $\text{Ba}_{1-x}\text{Sr}_x\text{TiO}_3$ sonogel and the well-isolated $\text{Ba}_{1-x}\text{Sr}_x\text{TiO}_3$ ($0 \leq x \leq 0.2$) single-crystal nanorods without any templates by controlling synthesis conditions. We also discuss the relationship between the forming conditions of sonogel and the nanorods' morphology.

2. Experimental section

The typical sample preparation of barium strontium titanate was as follows: 0.04 mol $\text{Ba}(\text{OH})_2 \cdot 8\text{H}_2\text{O}$ was dissolved in 0.3 mol acetic acid by ultrasonic radiation at room temperature. Then, a stoichiometric amount of $\text{Sr}(\text{CH}_3\text{COO})_2$ was introduced into above solution with sonication continued until a clear solution was formed. After that, the clear solution was transferred to a dried 60–70 ml of sonication glassware with an appropriate amount of tetrabutyl titanate dissolved in 12 ml ethanol and 5 ml benzene mixture. The high-intensity sonication was carried out by employing a direct immersion of titanium horn (diameter 1.05 cm, 20 kHz, $\sim 100 \text{ W/cm}^2$) into the glassware for 20–40 min in ice water bath (0°C) until a clear solution was formed again. Then, the solution was stored in for 3 h and the viscosity of the mixture enhanced, which result in the transformation of the mixture from liquid to transparent gel. The sonogel was then dried at 80°C under vacuum and grind for a while. After that, the gel powder was calcinated at different temperatures in air atmosphere controlling the velocity of thermoregulation.

The final products were characterized by various techniques. X-ray powder diffraction (XRD) was carried out on a Philips X'pert PRO super machine at a scan rate of $0.05^\circ/\text{s}$ using Cu K_α radiation (0.1541761 nm). The transmission electron microscopy (TEM) images were taken on a JEOL JEM-100SX TEM with an acceleration voltage of 100 kV. The high-resolution transmission electron microscopy (HRTEM) images were obtained with a JEOL-2010 microscopy at an acceleration voltage of 200 kV. Thermogravimetric analysis (TGA) and differential thermal analysis (DTA) were carried out on a Netzsch STA-409c Thermal Analyzer under air flow at a rate of $10^\circ\text{C}/\text{min}$.

3. Results and discussion

Fig. 1 shows the TG–DTA curves of typical $\text{Ba}_{0.8}\text{Sr}_{0.2}\text{TiO}_3$ gel dried at 80°C . These curves demonstrate the weight loss of the gel and the possible phase transition temperature. From the TG–DTA curves, the heat-treatment process could be divided into three steps which include the volatilization of water and organic compounds with low boiling point, thermal decomposition of organic ligands, and new phase formation of barium strontium titanate. The first endothermal weight loss of about 2.45% appears in the range of temperature below 300°C . This is assigned

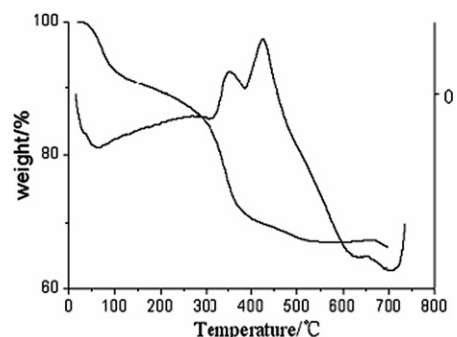


Fig. 1. TG–DTA curves of the $\text{Ba}_{0.8}\text{Sr}_{0.2}\text{TiO}_3$ sonogel dried at 80°C .

to the volatilization of water and organic compounds entrapped in the polymerized gel as well as the combustion of partial organic compounds with relative high boiling point. The second weight loss of about 4.5% happens at the temperature between 300°C and 500°C , among which there are two thermal acromions at 330°C and 398°C , respectively. They are supposed to be the results of both endotherm and exotherm which are caused by further weight loss of the combustion and exothermal reaction between different components. When the temperature is above 450°C , there is a third loss of weight. A broad exothermic peak appears, which implies the formation of a new phase.

The XRD patterns of the as-synthesized sample $\text{Ba}_{0.8}\text{Sr}_{0.2}\text{TiO}_3$ which was irradiated for 40 min are presented in Fig. 2. The XRD evolution indicates such system of gel is amorphous after being calcinated at the temperature below 500°C . Furthermore, the mixed phases of titania labeled by \bullet and barium strontium carbonate \triangle are observed at the temperature below 500°C . It is evident that the $\text{Ti}(\text{Obu-}n)_4$ has been decomposed into titania. When the temperature is further elevated to 600°C , the X-ray diffraction pattern is exactly like the pure barium strontium titanate pattern, which belongs to the cubic crystal structure as shown in Fig. 3(a). This crystallizing temperature of BST is lower than the previously reported 700°C [28,29]. The XRD card has demonstrated that tetragonal

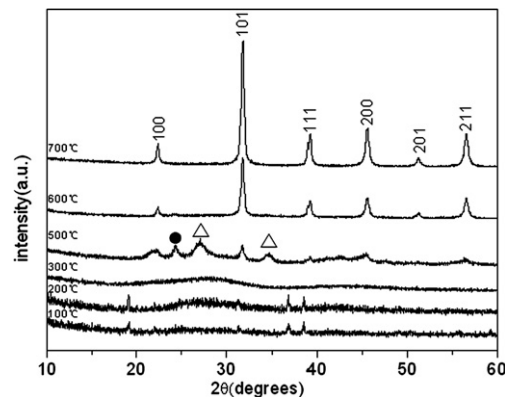


Fig. 2. The XRD patterns of $\text{Ba}_{0.8}\text{Sr}_{0.2}\text{TiO}_3$ sonogel calcinated for 12 h at different temperatures after being irradiated for 40 min.

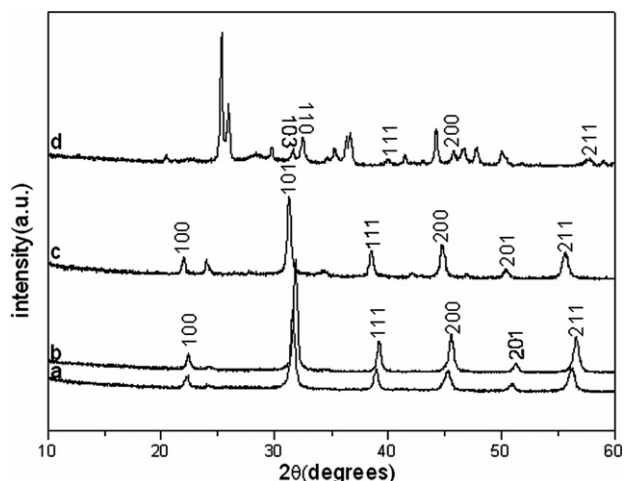


Fig. 3. The XRD patterns of the stoichiometric $\text{Ba}_{1-x}\text{Sr}_x\text{TiO}_3$ sonogel calcinated for 12 h at 600°C after being irradiated for 40 min. (a) $x = 0.1$; (b) $x = 0.2$; (c) $x = 0.5$ and (d) $x = 1$.

structure of pure barium titanate has a diffraction peak of 111 when 2θ ranges from 38° to 40° , two diffraction peaks of 002 and 200 from 44.9° to 45.4° . Because the atomic weight of strontium is smaller than barium, after part of barium is substituted by strontium, the parameter ratio c/a of tetragonal crystal cell may become smaller, which will further affect the diffraction peak. Therefore, except the peak of 111 is not changed, the substitution has caused the overlapping of 002 and 200 peaks, and thus we can only see 200/002 diffraction peak at 45.4° as shown in Fig. 2 at 600°C and 700°C [30,31]. Fig. 3 shows the powder X-ray diffraction patterns of $\text{Ba}_{1-x}\text{Sr}_x\text{TiO}_3$ sonogel which was calcinated at 600°C for 12 h after being irradiated for 40 min. The information from the patterns indicates only gel with $x \leq 0.2$ can form homogeneous cubic structural barium strontium titanate (as shown in Fig. 3(b) $\text{Ba}_{0.8}\text{Sr}_{0.2}\text{TiO}_3$), whereas gel with $x > 0.2$ can hardly form pure cubic structural products (as shown in Fig. 3(c) $\text{Ba}/\text{Sr} = 1:1$ and Fig. 3(d) $\text{Ba}/\text{Sr} = 0:1$).

Fig. 4 presents the TEM micrograph of the perovskite BST with a well-isolated rod like morphology when the gel was calcinated at 600°C for 12 h after being irradiated for 40 min. The diameters and lengths are about 70–100 nm and 650–1000 nm. Fig. 4(b) is the SAED pattern

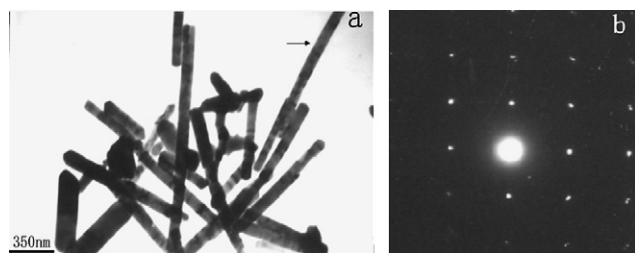


Fig. 4. (a) TEM image of $\text{Ba}_{0.8}\text{Sr}_{0.2}\text{TiO}_3$ nanorods which was prepared by ultrasonic radiation for 40 min and heat-treated for 12 h at 600°C . (b) The selected area electron diffraction pattern.

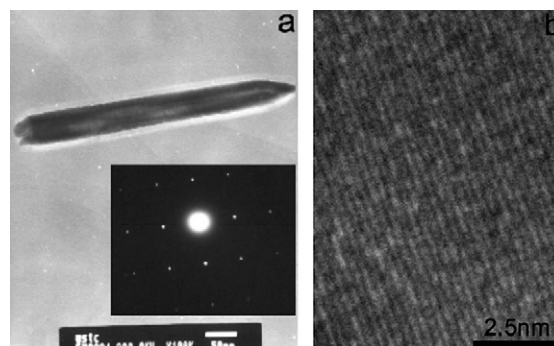


Fig. 5. (a) HRTEM image of $\text{Ba}_{0.8}\text{Sr}_{0.2}\text{TiO}_3$ nanorods and its selected area electron diffraction pattern. (b) The fringing spacing.

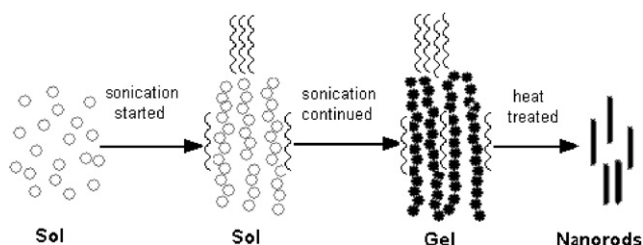
of the nanorod, which reveals that the BST products exhibit a cubic perovskite single-crystal structure. Fig. 5 is the HRTEM image of the nanorod above and its fringing spacing. According to the HRTEM image, well-resolved lattice fringes can be seen clearly, which give further information on fine micro-structure of the rod-like $\text{Ba}_{0.8}\text{Sr}_{0.2}\text{TiO}_3$.

In the ultrasound-assisted sol/gel process, it was found that ultrasound time in the preparation of sonogel is important to the morphology of products. To further investigate the influence of ultrasound time on the formation of typical $\text{Ba}_{0.8}\text{Sr}_{0.2}\text{TiO}_3$ nanorods, contrast experiment was carried out by reducing the ultrasound time to 20 min and 0 min, but other conditions were kept constant. $\text{Ba}_{0.8}\text{Sr}_{0.2}\text{TiO}_3$ gel which was prepared by ultrasonic radiation for 20 min and heat-treated for 12 h at 600°C is illustrated in Fig. 6(a) and (b). The result demonstrates that the morphology is different from the nanorods presented in Fig. 5. In this structure, the nanorods are composed of mutually connected spherical nanoparticles. A close observation of the nanorods will reveal that with the extension from the middle to the poles, the sizes of the particles become smaller and smaller. Fig. 6(c) is the TEM image of $\text{Ba}_{0.8}\text{Sr}_{0.2}\text{TiO}_3$ gel which was heat-treated for 12 h at 600°C without ultrasonic irradiation. It can be seen that $\text{Ba}_{0.8}\text{Sr}_{0.2}\text{TiO}_3$ without ultrasonication is composed of agglomerated particles. The results indicate that ultrasound power is vital to the nucleation of $\text{Ba}_{0.8}\text{Sr}_{0.2}\text{TiO}_3$ crystals and the rod like morphology. The possible formation mechanism is schematically illustrated in Scheme 1.

The formation of line structure of the sol and the subsequent nanorods could be attributed to three factors. First, the ultrasound cavitation bubbles create shock wave, which generates high local temperature and pressure during the process of formation and implosive collapse of bubbles. The molecules of the reaction mixture within the bubbles such as $\text{Ba}(\text{CH}_3\text{COO})_2$, $\text{Ti}(\text{O}i\text{Bu})_4$, $\text{Sr}(\text{CH}_3\text{COO})_2$ are fractured, forming highly reactive free radicals, which may also react with certain radical scavengers of $-\text{O}-\text{Ti}-\text{O}-$ or CH_3COO^- in the solution and thereby result in weakly colloid nucleation of $\text{H}_3\text{CCOO}-\text{Ba}-\text{O}-\text{Ti}-\text{O}-\text{Ba}-\text{OOCCH}_3$ or others [32]. Therefore, the preferential crystal nucleation will occur after heat-treatment and perhaps



Fig. 6. (a) TEM image of $\text{Ba}_{0.8}\text{Sr}_{0.2}\text{TiO}_3$ nanorods which was prepared by ultrasonic radiation for 20 min and heat-treated for 12 h at 600°C . (b) The magnified image. (c) TEM image of $\text{Ba}_{0.8}\text{Sr}_{0.2}\text{TiO}_3$ nanorods which were heat-treated for 12 h at 600°C without ultrasonic radiation.



Scheme 1. Schematic illustration of the formation of typical $\text{Ba}_{0.8}\text{Sr}_{0.2}\text{TiO}_3$ nanorods through the ultrasound-assisted sol/gel process.

results in the mutually connected spherical particles as shown in Fig. 6(b).

Second, in a homogeneous sol system, an acoustic wave travels along a straight line because the wave speed is constant everywhere in the sol [33]. Furthermore, the acoustic wave generated by the ultrasonic wave source is a kind of longitudinal wave. It enables the sol molecules to array in line along the direction of wave propagation (as shown in Scheme 1) [34].

Third, the hydrolytic-polymeric reaction of $\text{Ti}(\text{Obu-}n)_4$ leads to the formation of O–Ti–O long chain. The role of the power longitudinal ultrasound reinforces covalent bonds of O–Ti–O along the direction of wave propagation while weakens the covalent bonds along the transverse direction. This also makes it possible the preferential one-dimensional crystal growth in heat-treatment process and the resulting rod-like morphology.

As a result, when the ultrasonic time was reduced to 20 min, the sol system could not get enough ultrasound power to promote the preferential crystal nucleation and array the sol molecules in line. The nanorods will turn out the distinguishing morphology as shown in Fig. 6(a) and (b). When the ultrasonic time was reduced to 0 min, there was no ultrasound power to disperse and array the sol molecules. The resulting $\text{Ba}_{0.8}\text{Sr}_{0.2}\text{TiO}_3$ is composed of agglomerated nanoparticles after heat-treatment as shown in Fig. 6(c).

4. Conclusions

The monodispersed single-crystal barium strontium titanate nanorods have been prepared using barium hydroxide

$\text{Ba}(\text{OH})_2 \cdot 8\text{H}_2\text{O}$, strontium acetate $\text{Sr}(\text{CH}_3\text{COO})_2$, tetrabutyl titanate $\text{Ti}(\text{Obu-}n)_4$ as precursors via the simple combined method of ultrasonic-sol/gel. The diameters and lengths of typical resultant $\text{Ba}_{0.8}\text{Sr}_{0.2}\text{TiO}_3$ disperses between the range of 70–100 nm and 650–1000 nm, respectively. Sonochemical cavitation and ultrasonic time have important effect on the line structure of the as-prepared gel. This has an impact on further morphology of the nanorods.

Acknowledgement

This work is financially supported by BRJH of Chinese Academy of Science and Specialized Research Fund for the Doctoral Program of Higher Education (No. 20050358010).

References

- [1] A. Bachtold, P. Hadley, T. Nakanishi, C. Dekker, *Science* 294 (2001) 1313.
- [2] Z.W. Pan, Z.R. Dai, Z.L. Wang, *Science* 291 (2001) 1947.
- [3] C. Collier, T. Vossmeier, J. Heath, *Annu. Rev. Phys. Chem.* 49 (1998) 371.
- [4] Y. Gui, C. Lieber, *Science* 291 (2001) 851.
- [5] Y. Huang, X.F. Duan, Q.Q. Wei, C. Lieber, *Science* 291 (2001) 630.
- [6] J.G. Cheng, J. Tang, J.H. Chu, A.J. Zhang, *Appl. Phys. Lett.* 77 (2000) 1035.
- [7] J.H. Jeon, Y.D. Hahn, H.D. Kim, *J. Euro. Ceram. Soc.* 21 (2001) 1653.
- [8] J.H. Yoo, W. Gao, *J. Mater. Sci.* 34 (1999) 5631.
- [9] A. Catalan, S. Chang, R. Poisson, W. Baney, J. Benci, *J. Mater. Res.* 13 (1998) 1548.
- [10] B. Baumert, L. Chang, A. Matsuda, C. Tracy, N. Cave, R. Gregory, P. Fejes, *J. Mater. Res.* 13 (1998) 197.
- [11] S. Nenez, A. Morell, M. Pate, M. Maglione, J. Niepce, J. Ganne, *Euro. Ceram.* 206 (2002) 1513.
- [12] F. Selmi, F. Guerin, X. Yu, V.K. Varadan, V.V. Varadan, S. Komarneni, *Mater. Lett.* 12 (1992) 424.
- [13] V. Berbenni, A. Marini, *Z. J. Chem. Sci.* 57 (2002) 859.
- [14] L. Wu, Y.C. Chen, L.J. Chen, Y.P. Chou, Y.T. Tsai, *Jap. J. Appl. Phys.* 38 (1999) 5612.
- [15] T. Noh, S. Kim, C. Lee, *Bull. Kor. Chem. Soc.* 16 (1995) 1180.
- [16] Y. Kholam, S. Bhoraskar, S. Deshpande, H. Potdar, N. Pavaskar, S. Sainkar, S. Date, *Mater. Lett.* 57 (2003) 1871.
- [17] S. Krupanidhi, C. Peng, *Thin Solid Films* 305 (1997) 144.
- [18] M. McCormick, R. Roeder, E. Slamovich, *J. Mater. Res.* 16 (2001) 1200.
- [19] X.Z. Wei, N. Padture, *J. Ceram. Processing Res.* 5 (2004) 175.
- [20] D. Tahan, A. Safari, L. Klein, *J. Am. Ceram. Soc.* 79 (1996) 1593.
- [21] C. Kao, W. Yang, *Appl. Organomet. Chem.* 13 (1999) 383.

- [22] M. Zhang, Y. Bando, K. Wada, J. Mater. Sci. Lett. 20 (2001) 167.
- [23] S. Limmer, T. Hubler, G. Cao, J. Sol-Gel Sci. Tech. 26 (2003) 577.
- [24] L. Qiu, V.G. Pol, J. Calderon-Moreno, A. Gedanken, Ultrasonic Sonochem. 12 (2005) 243.
- [25] V.G. Pol, O. Palchik, A. Gedanken, I. Felner, J. Phys. Chem. B 106 (2002) 9737.
- [26] J. Urban, W. Yun, Q. Gu, H. Park, J. Am. Chem. Soc. 124 (2002) 1186.
- [27] D. Garcia, R. Guo, A. Bhalla, Integr. Ferroelectr. 42 (2002) 57.
- [28] M. Gust, L. Momoda, N. Evans, M. Mecartney, J. Am. Ceram. Soc. 84 (2001) 1087.
- [29] D. Tahan, A. Safari, L. Klein, J. Am. Ceram. Soc. 79 (1996) 1593.
- [30] H. Guo, Z. Zhang, B. Liu, X. Zhang, Acta Physico-Chimica Sinica 19 (2003) 1005.
- [31] Q. Lu, D. Chen, X. Jiao, J. Alloys Compd. 358 (2003) 76.
- [32] J.Z. Sostaric, R.A. Caruso-Hobson, P. Mulvaney, F. Grieser, J. Chem. Soc. Faraday Trans. 93 (1997) 179.
- [33] S.C. Wooh, L.M. Daniel, Ultrasonics 33 (1995) 3.
- [34] S. Biwa, A. Suzuki, N. Ohno, Ultrasonics 43 (2005) 495.